Evolution of microstructure and phases in *in situ* processed Ti–TiB composites containing high volume fractions of TiB whiskers

S.S. Sahay,[a] K.S. Ravichandran,[b] and R. Atri
Department of Metallurgical Engineering, 135 South 1460 East Room 412, The University of Utah,
Salt Lake City, Utah 84112

B. Chen and J. Rubin
Cercom Inc., 1960 Watson Way, Vista, California 97260

A series of titanium composites, with varying volume fractions of titanium monoboride (TiB) whiskers, were made by mixing various proportions of titanium (Ti) and titanium diboride (TiB_2) powders followed by hot pressing. The phases present were identified by x-ray diffraction. Microstructural examination revealed three different types of TiB whisker morphologies: (i) long and needle-shaped TiB whiskers that are isolated and randomly oriented in the Ti matrix at relatively low volume fractions (0.3), (ii) colonies of refined and densely packed TiB whiskers from intermediate-volume (0.55) to high volume (0.73 and 0.86) fractions, and (iii) coarse and elongated TiB particles with a few needle-shaped whiskers at the highest volume fraction (0.92). In all the composites, TiB was found to be the predominant reinforcement. However, in Ti–TiB composites with 0.86 and 0.92 volume fractions of TiB, a significant amount of TiB_2 was also present. The relative volume fractions of Ti, TiB, and TiB_2 phases were estimated from the integrated intensities of diffraction peaks by the direct comparison method employing the calculated structure factors and Lorentz polarization factors. The composite microstructure, as well as the evolution of different morphologies, of TiB whiskers is discussed.

I. INTRODUCTION

Titanium (Ti) matrix *in situ* composites are of considerable interest[1–3] for structural applications due to the potential for making composites with high specific stiffness and strength at low cost. The reinforcements are predominantly interstitial compounds such as TiC, TiB, TiN, and TiB_2. A survey of titanium phase diagrams[4] reveals that of all the possibilities including $Ti–TiB_2$, Ti–TiB, Ti–TiN, and Ti–TiC, Ti–TiB is the most attractive system from a number of perspectives. First, the absence of an intermediate phase and a narrow TiB stoichiometric range (49 to 50 at.% B; Fig. 1) makes the Ti–TiB system thermally stable at high temperatures compared with the other compounds, with the exception of TiB_2. However, because TiB is an intermediate phase in the $Ti–TiB_2$ system, the possibility of TiB formation at the $Ti–TiB_2$ interface as documented in several investigations[5,6] makes this system less attractive. Second, from

the mechanical behavior perspective, the whisker morphology of TiB,[2] the high elastic modulus of TiB (preliminary research[7] indicates that the elastic modulus of TiB is about 370 GPa), and the possibility of obtaining a significant increase in strength and deformation resistance due to TiB whisker-induced strengthening make the Ti–TiB composites even more attractive. There is only a small density difference between Ti and TiB (density of Ti is 4.5 g/cm^3 and that of TiB is 4.56 g/cm^3), making it possible to increase the TiB volume fraction (V_f) without affecting the density of the composite significantly. Additionally, the *in situ* Ti–TiB composites can be cost-effective compared with the fiber reinforced titanium composites, which require expensive fibers and costly fabrication steps.

Considerable research has been carried out on the Ti–TiB composites made by solidification. In particular, the boride morphologies,[8] crystallographic structure,[9] and mechanical behavior[10,11] have been studied. There are also studies showing that TiB can be formed in titanium alloys by combustion synthesis[12,13] and powder metallurgy cum extrusion.[14,15] These studies, however, are limited to composites with low volume fractions (0.3 or less) of TiB.
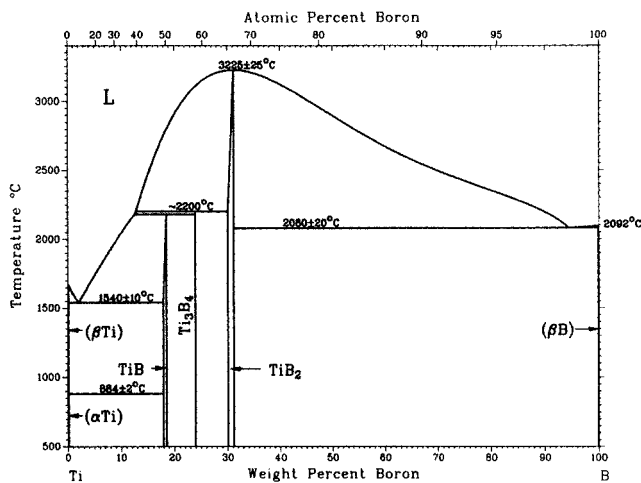
FIG. 1. Titanium–boron phase diagram.[4]

In the present study, *in situ* Ti–TiB composites processed in the solid state containing higher volume fractions of TiB were prepared by the hot pressing route. The emphasis is on high volume fraction levels ($\geqslant 0.3$) of TiB in the composite as well as creating solid TiB whiskers in the Ti matrix. This is in contrast to the TiB whiskers produced by solidification,[8,10] which exhibited a hollow interior due to shrinkage during transformation.[16] Detailed microstructural examination of the composites were performed. Identification of phases present in the composites was carried out by x-ray diffraction. The relative volume fractions of TiB were estimated from the integrated intensities of diffraction peaks by the direct comparison method.[17] The evolution of microstructure, phases, and the morphologies of TiB and TiB_2 phases are discussed.

II. EXPERIMENTAL PROCEDURE

A. Materials and characterization

In situ Ti–TiB composite plates of size 150 × 150 × 25 mm, with various volume fractions of TiB (Table I) reinforcements were fabricated by hot pressing Ti and TiB_2 powders using the Cercom PAD process (a proprietary process, Cercom Inc., Vista, CA). Mixtures of different volume fractions of Ti and TiB_2 powders were used to produce composites of various proportions of TiB phase, according to the reaction

$$Ti + TiB_2 \rightarrow 2TiB \quad . \quad (1)$$

Commercially available Ti powder (average particle size: 28 μm; composition in wt.%: 0.23% O, 0.02% N, 0.01% C, 0.04% Fe, and 0.024% H) and TiB_2 powder (average particle size: 2.4 μm; composition in wt.%: 30.3% B, 0.67% Zr, 0.01% C, 0.04% Fe, and 0.024% H) were used. The mixtures were prepared to produce the target compositions of 0.2, 0.4, 0.6, 0.8, and 1.0 volume

fractions of TiB in the Ti–TiB composites. The volume fractions of TiB_2 in the starting mixtures are given in Table I. A plate of monolithic Ti was also made by using the same starting Ti powder and the same processing technique for comparison. Cylindrical samples of about 5-mm diameter with the axis along the thickness direction of the fabricated plate were cut by electrodischarge machining (EDM). These samples were successively polished with 125-, 75-, 40-, 20-, and 10-μm perforated diamond disks. Final polishing was carried out with 6-, 1-, and 0.1-μm diamond pastes on a felt cloth. The samples were etched with Kroll's reagent. Microstructural examination was conducted in a scanning electron microscope (SEM) (Cambridge Instruments, Model: Stereoscan 240) by using secondary and back scattered electron imaging modes. X-ray diffraction analyses were carried out on metallographically polished specimens in a Siemens D5000 x-ray diffractometer operated at 40 kV and 40 mA and using Cu K_{α} radiation. A graphite monochromator, 0.1-mm detector slit size, and step size of $0.02°$ with 3 s per step were used.

B. Estimation of TiB volume fraction

The relative volume fractions of Ti and TiB phases were computed from the integrated intensities of selected peaks in the x-ray diffraction pattern by the direct comparison method.[17] This method can be applied to massive polycrystalline specimens. It has been widely used for measuring the amount of retained austenite in hardened steels. Basically, this method involves direct comparison of the integrated intensity of TiB line with the integrated intensity of Ti line. According to this method, the volume fraction of TiB (V_f) can be written as

$$V_f = \frac{R_{Ti} I_{TiB}}{R_{Ti} I_{TiB} + R_{TiB} I_{Ti}} \quad , \quad (2)$$

where I is the integrated intensity of the (*hkl*) peak. The parameter R is given by

$$R = \frac{|F_{hkl}|^2 pL}{V_o} \quad , \quad (3)$$

where V_o is the volume of unit cell, F_{hkl} is the structure factor, p is the multiplicity factor, and L is the Lorentz polarization factor.

TABLE I. Compositions of Ti–TiB composites.

TiB_2 in Ti–TiB_2 mixture (V_f)	Target composition TiB in Ti–TiB (V_f)	Actual composition Ti (V_f)	Actual composition TiB (V_f)	Actual composition TiB_2 (V_f)
0.118	0.2	0.7	0.3	0.00
0.237	0.4	0.45	0.55	0.00
0.355	0.6	0.27	0.73	0.00
0.474	0.8	0.08	0.86	0.06
0.592	1.0	0.00	0.92	0.08

III. RESULTS

A. X-ray diffraction analysis

The x-ray diffraction patterns for the different Ti–TiB composites, along with that of the pure Ti processed in the same way as the composites, are shown in Fig. 2. Hereafter, the composites are referred in terms of the actual volume fractions of phases present, as determined in this study, although the details of volume fraction determination are presented in the next section. The actual volume fractions of phases resulting after processing are given in Table I. The x-ray patterns in Fig. 2 indicate the presence of only Ti and TiB phases in composites of composition Ti–30TiB, Ti–55TiB, and Ti–73TiB. (The numbers before TiB and TiB_2 indicate the amount of respective phases in vol% determined from the analysis of x-ray diffraction patterns, as discussed in the next section.) In these composites, as the TiB volume fraction increased, the intensity of dominant Ti peaks [$(002)_{Ti}$, $(101)_{Ti}$] decreased and that of the dominant TiB peaks [$(200)_{TiB}$, $(201)_{TiB}$, $(210)_{TiB}$, and $(102)_{TiB}$ and $(312)_{TiB}$] increased. It is to be noted that the $(002)_{Ti}$ and $(111)_{TiB}$ peaks overlapped; therefore, the existence of a peak in this 2θ position may suggest the presence of either the Ti or the TiB phase. In the composite with a relatively high TiB volume fraction—that is, Ti–86TiB–6TiB$_2$—the TiB$_2$ phase was also present, as indicated clearly by the presence of dominant TiB$_2$ peaks such as $(001)_{TiB2}$ $(100)_{TiB2}$ and $(101)_{TiB2}$. The composite TiB–8TiB$_2$ consisted of only TiB and TiB$_2$ as indicated by the diffraction pattern. The relatively smaller unidentified peaks in this pattern could also be indexed on the basis of TiB$_2$ phase but are not shown. Although the starting compositions of both composites, Ti–86TiB–6TiB$_2$ and TiB–8TiB$_2$, were tailored to give only TiB, in addition to Ti if any (Table I), the presence of a significant amount of TiB$_2$ indicates the incompletion of the reaction ac-
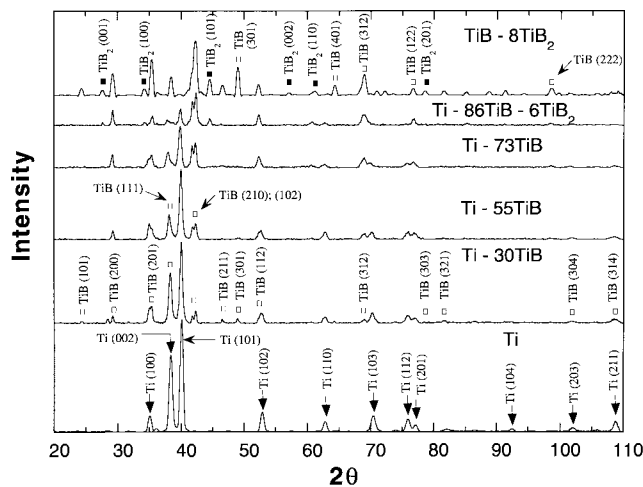
cording to Eq. (1). Therefore, the TiB$_2$ phase is the undecomposed part of the TiB$_2$ particles present before the reaction. It is to be noted that the Ti–86TiB–6TiB$_2$ and TiB–8TiB$_2$ composites did not contain any Ti$_3$B$_4$ phase (as evidenced the by lack of reflections in the patterns in Fig. 2), which is a phase intermediate between TiB and TiB$_2$ (Fig. 1). A study[18] identified the formation of Ti$_3$B$_4$ by peritectic reaction between TiB$_2$ and liquid at 2200 °C and its stability down to 1690 °C. However, in the present study, because the resolution of x-ray diffraction is restricted to typically about a few vol%, it is difficult to ascertain whether Ti$_3$B$_4$ is present or not, even in trace amounts, in these composites. Nevertheless, it is possible that Ti$_3$B$_4$ did not form in the present composites because of the relatively lower temperature of processing.

To estimate the volume fractions of phases, the structure factors along with the Lorentz polarization and multiplicity factors for different (*hkl*) planes were computed for Ti, TiB, and TiB$_2$ phases. The crystal structures[16,19] of TiB and TiB$_2$ phases are illustrated in Fig. 3. The lattice parameters and the fractional coordinates of atoms in TiB and TiB$_2$ are given in Table II. The structure factor, the multiplicity factor, and the Lorentz polarization factor were determined by using the information from a standard reference.[19] The calculated diffracted intensities (I_c) for different planes in Ti, TiB, and TiB$_2$ phases were then determined by the standard equation

$$I_c = |F_{hkl}|^2 pL \quad . \tag{4}$$

The values of the structure, Lorentz polarization, and multiplicity factors along with the computed intensities, normalized with respect to the plane with the highest
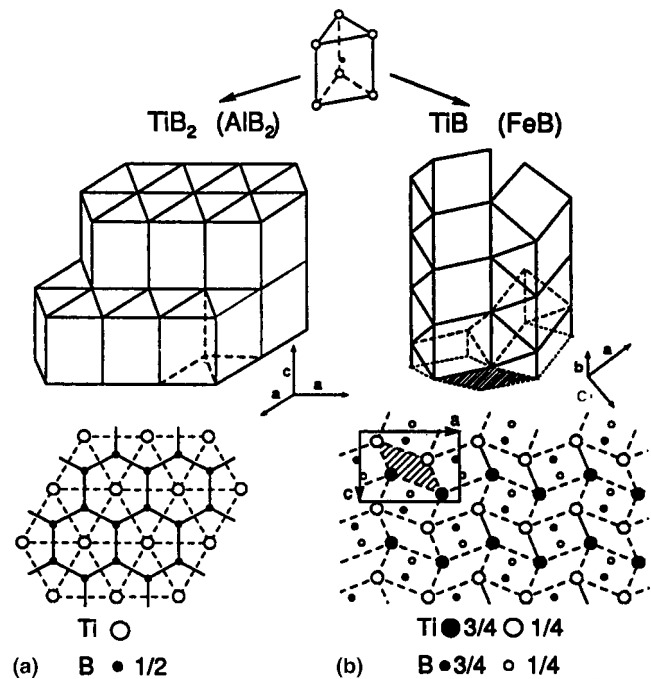

FIG. 2. X-ray diffraction patterns of Ti–TiB composites.

FIG. 3. Crystal structure of (a) TiB$_2$ and (b) TiB phases.[16,19]

TABLE II. Crystal structure, lattice parameters, and fractional coordinates in TiB and TiB_2.

Phase	Structure/space group	Unit cell (Å)	Atomic positions
TiB	Orthorhombic/Pnma	$a = 6.12$	Ti: 4c, m, $x = 0.177$, $y = 1/4, z = 0.123$
		$b = 3.06$	B: 4c, m, $x = 0.029$, $y = 1/4, z = 0.603$
		$c = 4.56$	
TiB_2	Hexagonal/P6/mmm	$a = 3.03$	Ti: 1a, 6/mmm, $x = 0$, $y = 0, z = 0$
		$c = 3.23$	B: 2d, $\bar{6}$m2, $x = 1/3$, $y = 2/3, z = 1/2$

intensity peak (I_{cTi}, I_{cTiB}, and I_{cTiB2}), are given in Table III through V for Ti, TiB, and TiB_2, respectively, along with the data taken from the Joint Committee for Powder Diffraction Standards (JCPDS) standard file. The normalized integrated intensities (I_{Ti}, I_{TiB}, and I_{TiB2}), measured from the x-ray diffraction patterns, are also included in these tables.

The data in Tables III through V indicate that the computed relative intensity levels agree reasonably well with the JCPDS standard. The differences between these two relative intensities were usually larger for the overlapping peaks in the diffraction pattern. Among the various Ti peaks (Table III), the $(101)_{Ti}$ peak is the strongest in all the samples, consistent with the JCPDS standard and the computed relative intensities. It should be noted that because $(100)_{Ti}$, $(002)_{Ti}$, $(102)_{Ti}$, and $(110)_{Ti}$ peaks overlapped with $(201)_{TiB}$, $(111)_{TiB}$, $(112)_{TiB}$, and $(401)_{TiB}$ peaks respectively, the relative intensities of these peaks in the diffractograms of the present composites are not included in Table III. The relative intensity value of $(002)_{Ti}$ is much higher compared with the computed and the JCPDS standard relative intensity values. This may suggest a preferred orientation in the Ti matrix. A similar behavior can be expected in the Ti–TiB composites, as the relative intensities of $(103)_{Ti}$ and $(112)_{Ti}$ peaks in the composites are nearly the same as that in monolithic Ti.

In the case of the TiB phase (Table IV), although the maximum value of computed relative intensity is for $(111)_{TiB}$, the JCPDS standard and the composites samples have intensity maxima for $(102)_{TiB}$. However, the relative intensities for most of the other planes in the composite samples are comparable to that of the JCPDS standard, indicating a nearly random nucleation and growth of TiB whiskers in the matrix. A random orientation of whiskers is expected during the *in situ* processing, especially when nucleation and growth of a phase in solid state in a matrix is involved. However, there were some exceptions, and these were mostly found in the data for the TiB–8TiB$_2$ composite (Table IV). In the case of TiB_2 (Table V), the maximum relative intensity corresponded to the $(101)_{TiB2}$ for the Ti–86TiB–6TiB$_2$ and TiB–8TiB$_2$ samples, and it agreed with the computed and the JCPDS standard data. However, the relative intensities for other peaks were either higher or lower than the computed or JCPDS data by as much as a factor of two. A resolution of the observed discrepancies between the experimentally observed relative intensities and the computed or JCPDS data may suggest preferred orientation, but a resolution of this aspect is beyond the scope of this study.

B. Volume fractions of phases

The reasonable agreement between the computed relative intensities and the JCPDS standard intensities indicates that the diffraction characteristics are similar to the monolithic materials. Therefore, it is possible to estimate the relative volume fractions of phases with reasonable accuracy. However, this requires accurate values of integrated intensities of the peaks in the diffractograms. Therefore, in Fig. 2, the intensity peaks that are strong and well separated from other peaks were selected for computation of relative volume fractions of various phases. The selected peaks were $(101)_{Ti}$, $(200)_{TiB}$, and $(101)_{TiB2}$. These peaks also exhibited good agreement between the computed, JCPDS standard and the intensi-

TABLE III. Normalized integrated x-ray line intensities for Ti peaks.

(hkl)	2θ	d (Å)	$\|F\|^2$	L	p	I_{cTi} computed	I_{Ti} in JCPDS	I_{Ti} in Ti	I_{Ti} in Ti–30TiB	I_{Ti} in Ti–55TiB	I_{Ti} in Ti–73TiB	I_{Ti} in Ti–86TiB–6TiB$_2$
(100)	35.10	2.555	249	19	6	25	30	13	*	*	*	*
(002)	38.44	2.340	927	16	2	25	26	68	*	*	*	*
(101)	40.19	2.242	670	14	12	100	100	100	100	100	100	100
(102)	53.06	1.725	173	8	12	14	19	20	*	*	*	*
(110)	63.02	1.474	582	5	6	16	17	12	*	*	*	*
(103)	70.73	1.331	386	4	12	16	16	21	21	17	16	...
(112)	76.37	1.246	474	4	12	17	16	17	19	26	21	...
(201)	77.40	1.232	350	3	12	13	13	8	10	14	*	...
(104)	92.72	1.064	96	3	12	3	3	4	...	...	...	...

*Overlapping peak.

ties from the diffractograms. The relative volume fractions of Ti, TiB, and TiB_2, computed by the direct comparison method [Eqs. (2) through (5)], are given in Table I. In the Ti–86TiB–6TiB$_2$ composite comprising three phases, the volume fraction of Ti, independently measured by quantitative metallography, was used in the determination of TiB and TiB_2 volume fractions.

C. Microstructure

Figures 4 through 8 illustrate the microstructure, the distribution, and the morphology of TiB phases in Ti–TiB composites Ti–30TiB, Ti–55TiB, Ti–73TiB, and Ti–86TiB–6TiB$_2$ as well as the TiB–TiB$_2$ composite TiB–8TiB$_2$. Figures 4(a) and 4(b) illustrate the microstructural details of the Ti–30TiB composite, as observed in the backscattered electron (BSE) imaging mode. The microstructures of the other composites were difficult to resolve in the BSE mode because of fine scale features; therefore, the secondary electron imaging (SEI) mode was used.

In the composite with a TiB volume fraction of 0.3, pristine TiB whiskers, randomly distributed in the Ti matrix [Figs. 4(a) and 4(b)] were observed. Although most of the whiskers were found to be solid, there were some that were hollow. This is in contrast to the solidification processed composites, where hollow cores in the TiB

whiskers, possibly due to shrinkage, were found.[9,10] The longest needle-shaped whiskers observed in this composite had a length of about 50 μm and a width of about 5 μm (aspect ratio ≈ 10). It is possible that a range of whisker lengths and widths occurred in this composite, because the whiskers were formed *in situ,* according to Eq. (1). The phase contrast observed in the Ti matrix [Fig. 4(b)] may be due to the phases formed due to the contamination by C, N, and O that were picked up during composite processing. (This is possible, because the processing was carried out using graphite dies and under back-filled argon of commercial purity that probably had traces of O_2 and N_2.) A detailed investigation of the matrix microstructure is beyond the scope of this study.

In the Ti–55TiB composite [Figs. 5(a) and 5(b)], two different types of TiB whisker morphologies were observed: (i) needle-shaped randomly oriented TiB whiskers in the Ti matrix [Fig. 5(a)] and (ii) colonies of densely packed short TiB whiskers [Fig. 5(b)]. The short TiB whisker colonies appear to be interconnected and uniformly distributed in the matrix. The long TiB whiskers had an average length of 40 μm and a width of 4.5 μm, whereas the dimensions of the agglomerated whiskers were about 1.4 μm long and about 0.6 μm wide. The aspect ratios of the primary TiB whiskers therefore are roughly the same as that in the Ti–30TiB composite.

TABLE IV. Normalized integrated x-ray line intensities for TiB peaks.

(hkl)	2θ	d (Å)	$|F|^2$	L	p	I_{cTiB} computed	I_{TiB} in JCPDS	I_{TiB} in Ti–30TiB	I_{TiB} in Ti–55TiB	I_{TiB} in Ti–73TiB	I_{TiB} in Ti–86TiB–6TiB$_2$	I_{TiB} in TiB–8TiB$_2$
(101)	24.50	3.633	170	42	4	16	20	15				12
(200)	29.25	3.053	936	29	2	30	32	47	36	32	36	40
(201)	35.29	2.543	1074	19	4	45	80	*	*	*	*	65
(111)	38.37	2.346	1426	16	8	100	80	*	*	*	*	34
(210)	41.80	2.161	2493	13	4	72	64	58	51	68	62	48
(102)	42.23	2.140	2922	13	4	83	100	100	100	100	100	100
(211)	46.42	1.956	819	10	8	37	40	30	...	...	...	17
(301)	48.89	1.863	1945	9	4	40	56	45	...	...	...	51
(112)	52.12	1.755	962	8	8	34	40	*	*	*	*	20
(401)	63.70	1.461	1239	5	4	14	28	*	*	*	*	9
(312)	68.95	1.362	1565	4	8	30	72	50	57	66	54	37

*Overlapping peak.

TABLE V. Normalized integrated x-ray line intensities for TiB_2 peaks.

| (hkl)	2θ	d (Å)	$|F|^2$	L	p	I_{cTiB2} computed	I_{TiB2} in JCPDS	I_{TiB2} in Ti–86TiB–6TiB$_2$	I_{TiB2} in TiB–8TiB$_2$
(001)	27.62	3.227	131	32	2	23	22	24	33
(100)	34.16	2.622	179	20	6	59	55	29	40
(101)	44.48	2.035	272	11	12	100	100	100	100
(002)	57.04	1.613	271	6	2	9	12	...	12
(110)	61.16	1.514	252	6	6	23	27	...	11
(201)	78.72	1.215	151	3	12	16	16	...	35
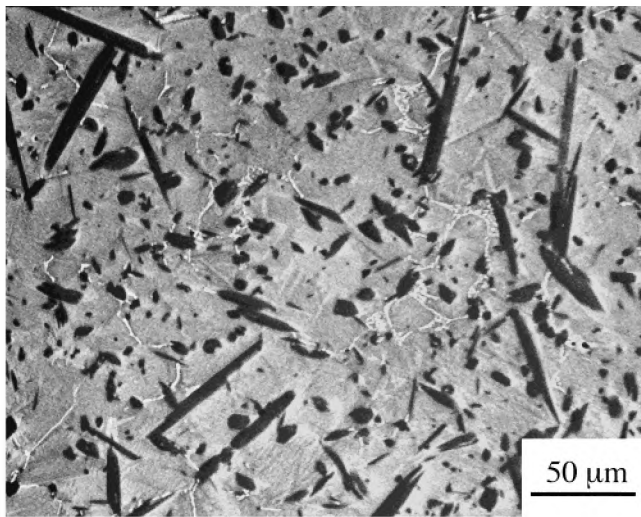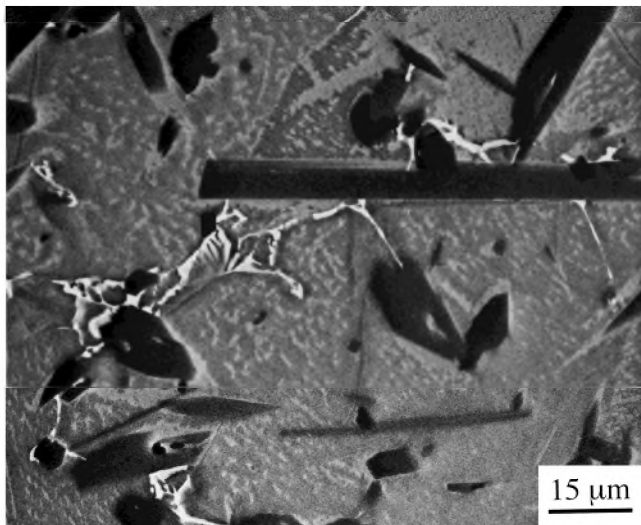
FIG. 4. (a) and (b) Microstructures of Ti–30TiB composite containing 30 vol% TiB.

The sizes and morphologies of TiB whiskers in the Ti–73TiB and Ti–86TiB–6TiB$_2$ composites (Figs. 6 and 7) were distinctly different from the other Ti–TiB composites. The Ti–73TiB composite consisted of TiB whiskers that were about 3 μm long and about 0.3 μm wide [Fig. 6(b)], indicating pronounced refinement (by about a factor of 10) in size, compared with the Ti–30TiB and Ti–55TiB composites. The whiskers also appear to be interconnected to some degree. The Ti–86TiB–6TiB$_2$ composite also had similar whisker morphology [Fig. 7(b)]. In both these composites, the size range of the TiB whiskers was narrow and the distribution was relatively more uniform. It is to be noted that in the Ti–86TiB–6TiB$_2$ composite, the presence of about 6 vol% of TiB$_2$ was detected by the x-ray diffraction, indicating that the reaction according to Eq. (1) was incomplete in this composite.
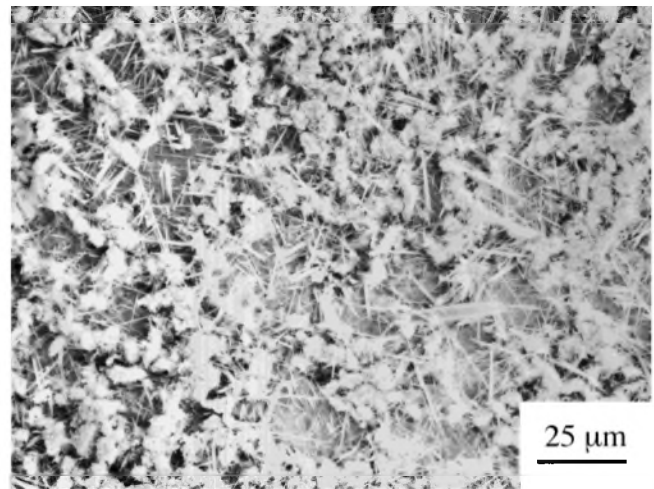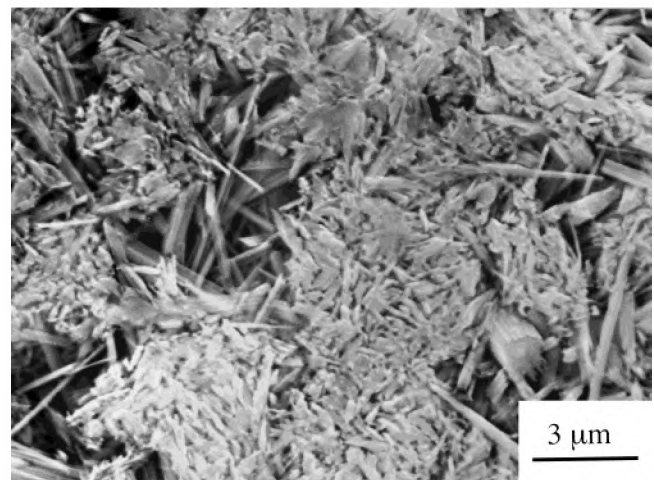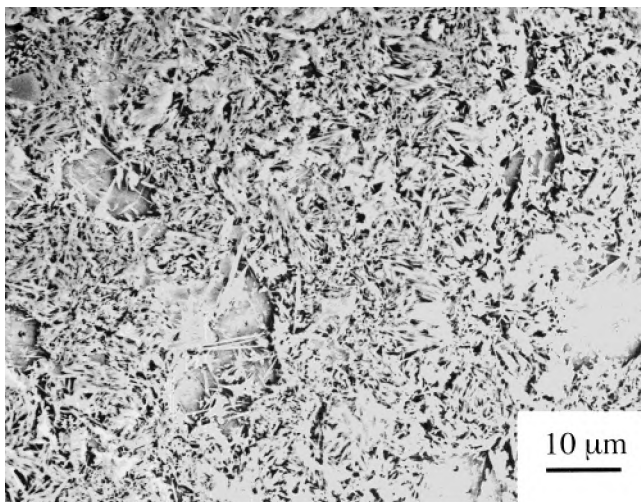

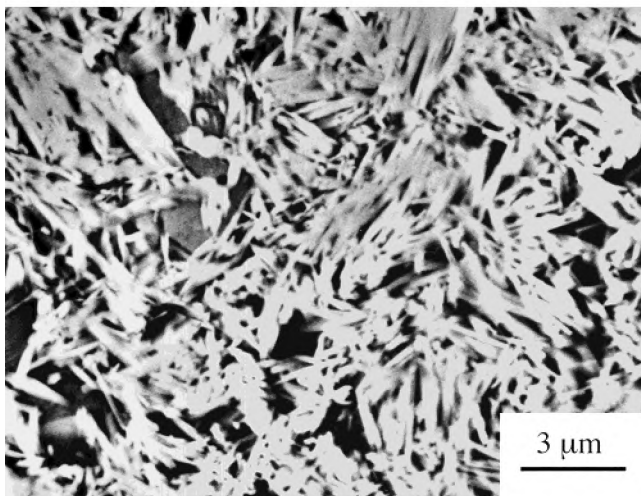FIG. 5. (a) and (b) Microstructures of Ti–55TiB composite containing 55 vol% TiB.

The microstructure of the composite with the highest TiB volume fraction—namely, TiB–8TiB$_2$—showed pronounced coarsening of whiskers [Figs. 8(a) and 8(b)], and it is composed of only TiB and TiB$_2$ phases. The TiB whisker size distribution was found to be wide, unlike the Ti–73TiB and Ti–86TiB–6TiB$_2$ composites. The whiskers in this composite had sizes up to 20 μm in length and 5 μm in width, suggesting that the average aspect ratio ($\approx$4) was considerably smaller than that observed in other composites. There was also a significant amount (8 vol%) of unreacted TiB$_2$ particles, which can be seen as coarse, nearly spherical particles in the microstructure [Fig. 8(b)].

IV. DISCUSSION

The formation of TiB with varied morphologies as well as the retention of unreacted TiB$_2$ in the high volume fraction TiB composites can be understood in
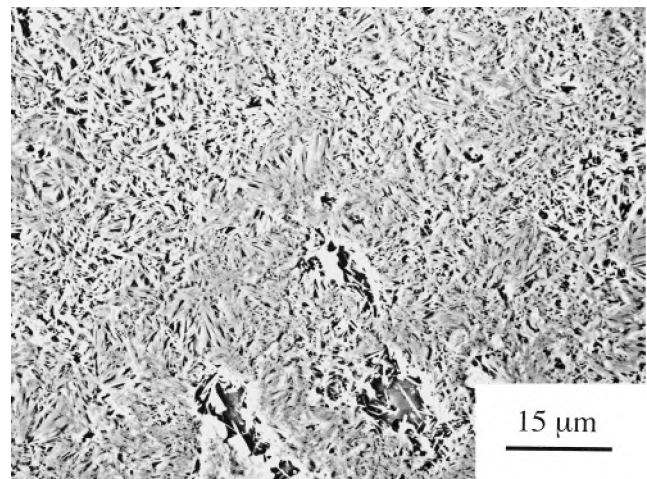
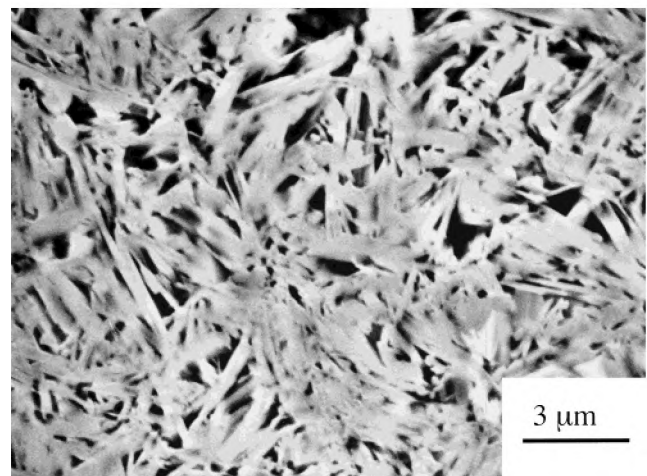FIG. 6. (a) and (b) Microstructures of Ti–73TiB composite containing 73 vol% TiB.

FIG. 7. (a) and (b) Microstructures of Ti–86TiB–6TiB$_2$ composite containing 86 vol% TiB and 6 vol% TiB$_2$.

light of the crystal structure (more importantly the atomic arrangements in the lattice) of TiB, diffusion of B in TiB as well as the relative volume fractions, and the spatial arrangement of Ti and TiB$_2$ powder particles in the starting mixture.

First, it is relevant to discuss the crystal structures of TiB and TiB$_2$ phases. The crystal structure, lattice parameters, and fractional coordinates of TiB and TiB$_2$ phases are given in Table II. The crystal structures of TiB and TiB$_2$ phases are illustrated in Fig. 3. The structure of TiB and TiB$_2$ phases are based on the same building block: the trigonal prismatic array of six Ti atoms with a B atom in the center.[16,19] In TiB$_2$, the prismatic building blocks are in a closed packed array, sharing all their faces with the neighboring prisms [Fig. 3(a)]. The TiB structure is formed by closed packing of the trigonal prisms only in one direction, forming columns with a rectangu-

lar base with the central chain of B atoms oriented in the [010] direction of the crystal. These columns are connected to each other only along the edges, which are parallel to the [010] direction. A B-free "pipe" surrounded by metal atoms is formed and its parallelogram-shaped cross section is made up of four neighboring columns containing B chains, as shown in Fig. 3(b).

Second, the variations in the morphology and the relative proportions of phases in the reacted composite can depend on B diffusion, besides the starting proportions of Ti and TiB$_2$ particles and their spatial arrangement in the starting mixture. Several investigations[6,13,16] indicate that TiB forms as whiskers with a high aspect ratio with the orientation relationship between TiB and α–Ti as described by

$$(100)_{TiB} \| (0001)_{\alpha-Ti} \quad ; \quad [010]_{TiB} \| [11\bar{2}0]_{\alpha-Ti} \quad , \quad (5)$$

with the $[010]_{TiB}$ direction parallel to the axis of the whiskers. The growth of the whiskers has been primarily
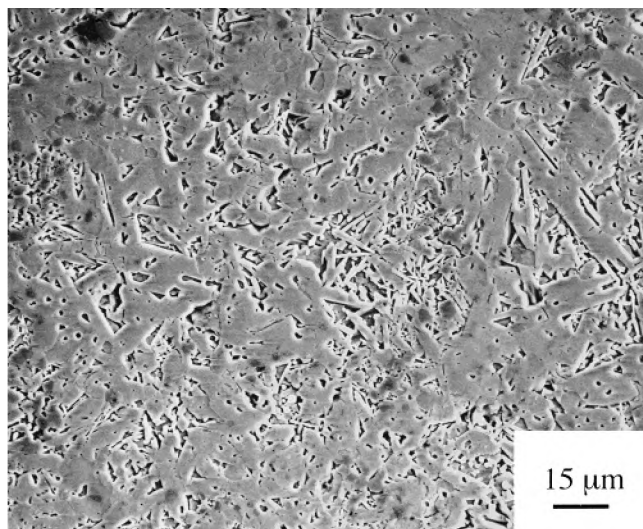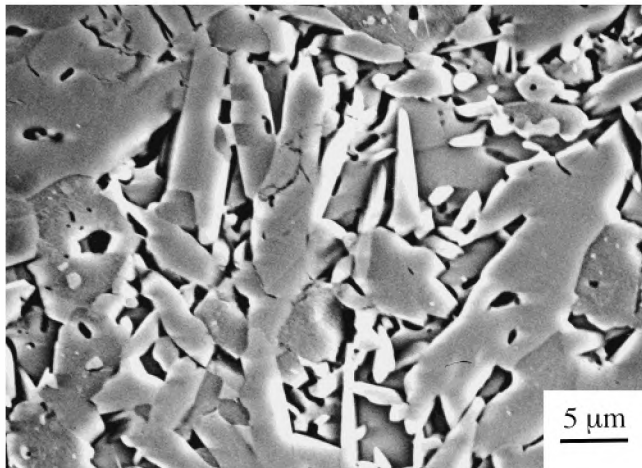
FIG. 8. (a) and (b) Microstructures of TiB–8TiB$_2$ composite containing 92 vol% TiB and 8 vol% TiB$_2$.

attributed to the one-way diffusion of B along [010]$_{TiB}$, the rate of which was suggested[6,16] to be much higher than that of the opposite diffusion of Ti in TiB. Additionally, apart from the diffusion-enhanced growth rate, because of the continuous and zigzag arrangement of B atoms[16,19] as well as the higher density of strong B–B bonds in the [010] direction, the growth rates in this direction can be higher, relative to the [100], [101], and [001] directions. Therefore, it can be inferred that the growth rate of TiB whiskers in the Ti matrix in the axial direction can be higher than that in the transverse direction. This is also consistent with the relatively higher values of the estimated diffusivities of B in TiB compared with that in TiB$_2$, even though the calculated activation energies for B diffusion in TiB and TiB$_2$ are nearly the same.[6] As a result, TiB exhibits a whisker morphology bound by slower growing planes in transverse directions.

The mechanism of formation of TiB whiskers with different morphologies in the low volume fraction and the high volume fraction TiB composites can be explained with the aid of Figs. 9(a) through 9(f). For example, in the low TiB volume fraction composite, the Ti particles would be surrounded by TiB$_2$ particles [Fig. 9(a)] after initial compaction. Because the TiB$_2$ particle size is about one-tenth that of the Ti particles, the TiB$_2$ particles would occupy the interstitial spaces between Ti particles, according to the packing theories for bimodal particle sizes.[20,21]

Therefore, the mean-free-path (MFP) in Ti can then be expected to be of the order of Ti particle size. Growth of TiB whiskers into the Ti matrix with B diffusion along the [010] direction can then proceed without hindrance [Fig. 9(b)] until complete decomposition of TiB$_2$ or blocking by other whisker growing from neighboring TiB$_2$ particles [Fig. 9(c)]. In the Ti–30TiB composite, the degree of blocking by other TiB whiskers appears to be small (Fig. 4), leading to largely isolated high aspect ratio whiskers.

Theoretically, at a critical TiB$_2$ volume fraction— for instance, about 29 vol%—TiB$_2$ particles can be expected to completely surround the Ti particles, because, according to bimodal particle packing theories,[20,21] more efficient packing of powder particles in the mixture would occur at about this vol%, for the size ratios of powders used in the present study. In this condition, the available MFP for the TiB growth is lower than that in the Ti–30TiB composite, because TiB whiskers growing simultaneously from TiB$_2$ particles across the Ti particle would impede each other. The particle arrangement in 55TiB and 73TiB composites are close to this spatial configuration [Fig. 9(d)]. This means that, in these composites, the TiB whiskers can grow to lengths that are only fractions of the Ti particle size before they are impeded by the other TiB whiskers growing from the neighboring TiB$_2$ particles [Fig. 9(e)]. However, because the reaction given by Eq. (1) is incomplete at this stage, further formation of TiB is possible only by the diffusion of B or Ti in the transverse direction of the TiB whiskers already formed or by the formation of new TiB whiskers. Although the former mechanism can lead to thickening of TiB whiskers, the latter mechanism can lead to formation of new and relatively finer whiskers. If both mechanisms occur to some extent, then the creation of new whiskers and lumping or connecting of these whiskers is possible. However, because the B diffusion in the transverse direction is much lower than that in the longitudinal direction, new whisker growth is rapid compared with the thickening of the whiskers already formed [Fig. 9(f)]. This mechanism appears to reasonably explain the microstructural morphologies observed in the high volume fraction composites—
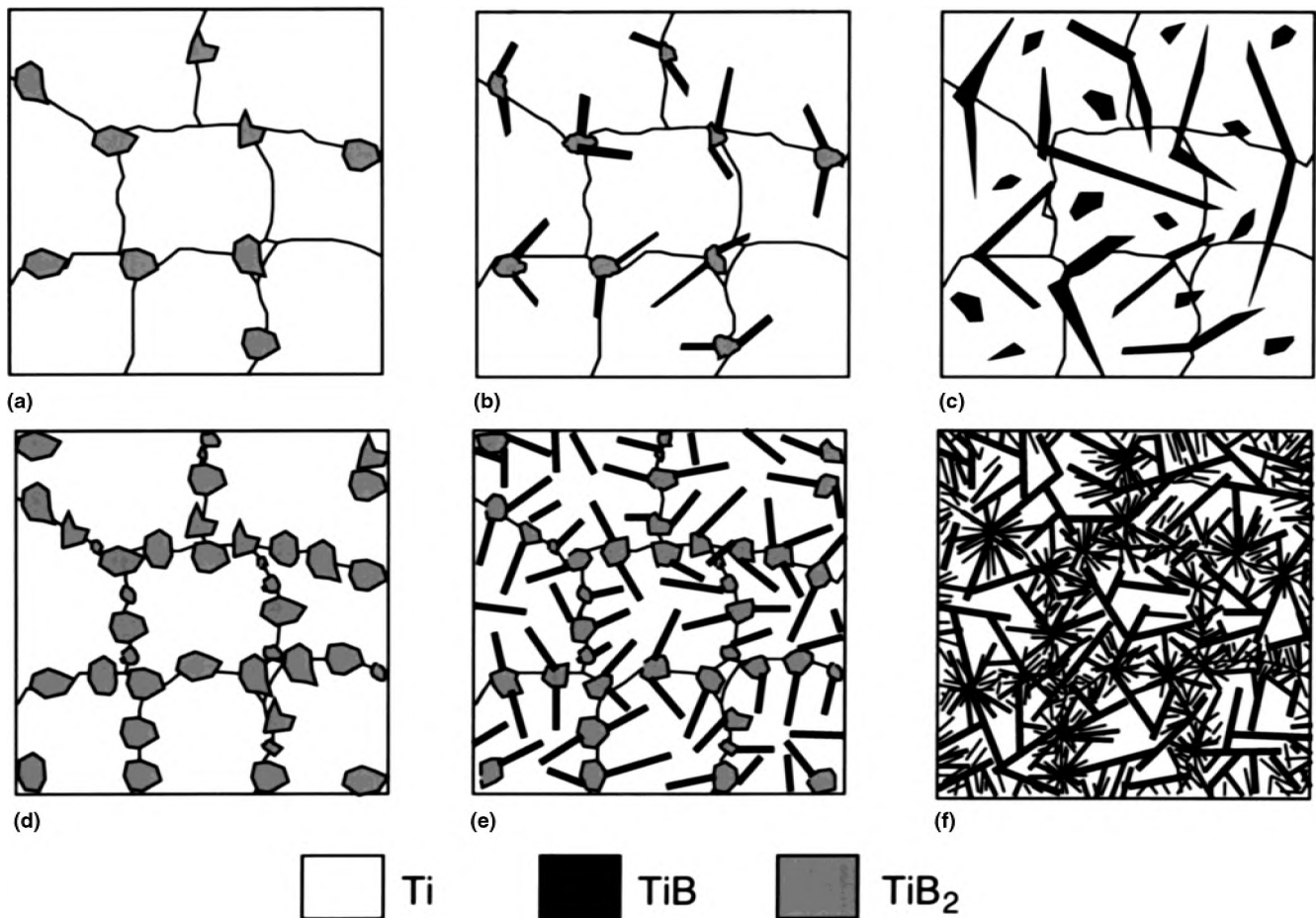
FIG. 9. Schematics describing development of TiB whisker morphologies in Ti–TiB composites: (a) through (c) for the use of low volume fraction ($\approx$10 vol%) TiB_2 particles in the starting mixture, and (d) through (f) for the case of starting mixture with a critical volume fraction ($\approx$29 vol%) of TiB_2 particles corresponding to efficient packing of bimodal particle sizes.

Ti–73TiB (Fig. 6) and Ti–86TiB–$6TiB_2$ (Fig. 7)—relative to the morphologies observed in Ti–55TiB composite (Fig. 5).

The morphological differences between Ti–55TiB and Ti–73TiB as well as Ti–86TiB–$6TiB_2$ can be explained on the basis of whether the TiB_2 volume fraction is less or more than the critical volume fraction (29%) for efficient particle packing in a bimodal distribution of particle sizes. In the Ti–55TiB composite with 23.7% TiB_2 in the starting mixture, the MFP of the first set of whiskers can be expected to be longer than the Ti particle diameter [Fig. 5(a)]. After formation of the first set of whiskers, the remaining TiB_2 particles appear to transform into groups of short TiB whiskers, as shown in Fig. 5(b). The locations of these groups appear to belong to that of the TiB_2 particles that existed before reaction, consistent with the above hypothesis. On the other hand, in the Ti–73TiB and Ti–86TiB–$6TiB_2$ composites, the TiB_2 volume fractions are higher than 29% (35.5 and 47.4, respectively). In addition to the surrounding of Ti particles by more TiB_2 particles, the number of particles

located between Ti particles are also more relative to that of Ti–30TiB and Ti–55TiB composites. Therefore, the whisker lengths can be expected to be shorter because of the reduced MFP caused by the simultaneous growth of more TiB whiskers. Subsequently, the growth of secondary TiB whiskers will be promoted by the remnant TiB_2. One can then envisage the growth of successively shorter whiskers until the TiB_2 completely converted, resulting in a high density of fine and short whiskers, as illustrated in Fig. 9(f). This hypothesis is supported by the colonies of whiskers observed in Ti–73TiB and Ti–86TiB–$6TiB_2$ composites (Figs. 6 and 7).

At the highest volume fraction (59.2%) of TiB_2 in the starting mixture, even more particles would surround the Ti particles, with the increased probability of TiB_2 particles surrounding the other TiB_2 particles in regions between the Ti particles. This can lead to even further reduction in MFP in Ti, leading to the observation of only a few long TiB whiskers [Fig. 8(b)] in the TiB–$8TiB_2$ composite. Because the growth in the length direction is geometrically limited at an early stage of

reaction, growth in the transverse direction is possible, leading to the thickening and the reduction in the aspect ratio of the TiB whiskers. Because the transverse B diffusion is relatively slower, the rate of conversion of TiB_2 into TiB also will be lower. In addition, the presence of unreacted TiB_2 is likely also due to the fact that some TiB_2 particles are not in direct contact with Ti particles according to the bimodal packing arrangement[20,21] at this volume fraction. The presence of a significant amount of unreacted TiB_2 (Fig. 2) in this composite as well as in the Ti–86TiB–6TiB_2 composite can be explained on the basis of this reasoning. The Ti–30TiB, Ti–55TiB and Ti–73TiB composites are the only ones in which the reaction according to Eq. (1) occurred through complete conversion of TiB_2 into TiB under the processing conditions.

V. CONCLUSIONS

(1) Ti–TiB composites with different volume fractions of TiB were fabricated *in situ* by hot pressing Ti and TiB_2 powders. In all the composites, TiB was the predominant boride phase. The composites with a relatively high TiB content also revealed the presence of an unreacted TiB_2 phase. No evidence for the presence of a Ti_3B_4 phase in excess of the resolution of the x-ray diffraction technique under the processing conditions of this study was found.

(2) The measured x-ray integrated intensities of various planes of Ti, TiB, and TiB_2 phases agreed reasonably well with the computed data and the JCPDS standard data. The comparable nature of the relative intensities of different TiB peaks with the corresponding peaks in the JCPDS standard indicated the random nucleation and growth of TiB in the microstructure. The volume fractions of TiB phase in the composites were determined from the integrated intensities by the direct comparison method.

(3) Microstructures of the Ti–TiB composites indicated a change in morphology from long, needle-shaped and randomly oriented TiB whiskers at low TiB volume fractions (0.3) to short, agglomerated TiB whiskers in the composites with intermediate (0.55) to high TiB volume fractions (0.73 and 0.86). In the composite with the highest TiB volume fraction (0.92), significant thickening and a reduction in the aspect ratio of the TiB whisker was observed.

(4) A mechanism on the basis of crystallography of TiB preferential diffusion of B in the axial direction of TiB whiskers and the bimodal packing arrangement of Ti and TiB_2 particles in the starting mixture is suggested for formation of varied morphologies in different composites.

REFERENCES

1. M.X. Thompson and V.C. Nardone, Mater. Sci. Eng. **A144,** 1221 (1991).
2. F.W. Crossman and A.S. Yue, Metall. Trans. **1A,** 1545 (1971).
3. J.J. Valencia, J.P.A. Lofvander, C. McCullough, C.G. Levi, and R. Mehrabian, Mater. Sci. Eng. **A144,** 25 (1991).
4. *Binary Alloy Phase Diagram, ASM Handbook,* edited by H. Baker (ASM International, Materials Park, OH, 1992), Vol. 3, p. 2.85.
5. A.G. Metcalfe, in *Metal Matrix Composites,* edited by L.J. Broutman and R.H. Krock (Academic Press, New York, 1974), Vol. 1, p. 65.
6. Z. Fan, Z.X. Guo, and B. Cantor, Composites **28A,** 131 (1997).
7. R. Atri, K.S. Ravichandran, and S.K. Jha, Acta Mater. (1998, in press).
8. M. De Graef, J.P.A. Lofvander, C. McCullough, and C.G. Levi, Acta Metall. Mater. **40,** 3395 (1992).
9. M. D. Graef, J.P.A. Lofvander, and C.G. Levi, Acta Metall. Mater. **39,** 2381 (1991).
10. J.A. Philliber, F.C. Dary, F.W. Zok, and C.G. Levi, in *Recent Advances in Titanium Metal Matrix Composites,* edited by F.H. Froes and J. Storer (The Minerals, Metals and Materials Society, Warrendale, PA, 1995), p. 213.
11. J.A. Philliber, F.C. Dary, F.W. Zok, and C.G. Levi, *Titanium '95 Science and Technology,* edited by P.A. Blenkinsop, W.J. Evans, and H.M. Flower (The Institute of Materials, London, 1996), Vol. 3, p. 2714.
12. W.Y. Wang, H.C. Yi, and A. Petric, Metall. Mater. Trans. **29A,** 3037 (1995).
13. T. Yamamoto, A. Otsuki, K. Ishihara, and P.H. Shingu, Mater. Sci. Eng. **A239/240,** 647 (1997).
14. D.X. Li, D.H. Ping, Y.X. Lu, and H.Q. Ye, Mater. Lett. **16,** 322 (1993).
15. T. Saito, H. Takamiya, and T. Furata, in *Titanium '95 Science and Technology,* edited by P.A. Blenkinsop, W.J. Evans, and H.M. Flower (The Institute of Materials, London, 1996), Vol. 3, p. 2859.
16. M.E. Hyman, C. McCullough, J.J. Valencia, C.G. Levi, and R. Mehrabian, Metall. Trans. **22A,** 1647 (1991).
17. B.D. Cullity, *Elements of X-Ray Diffraction,* 2nd ed. (Addison-Wesley, Reading, MA, 1978).
18. K.E. Spear, P. McDowell, and F. McMahon, J. Am. Ceram. Soc. **69,** C-4 (1986).
19. B.F. Decker and R. Kasper, Acta Crystallogr. **7,** 77 (1954).
20. R.K. McGeary, J. Am. Ceram. Soc. **44,** 513 (1961).
21. J.V. Milewski, in *Proceedings of the 29th Annual Technical Conference* (Reinforced Plastics/Composites Institute, The Society of Plastics Industry, Inc., Washington, DC, Section 10-B, 1974), p. 1.